Chemistry–A European Journal
Research Article
doi.org/10.1002/chem.202403555
Chemistry Europe
European Chemical Societies Publishing
www.chemeurj.org

Heavier Diferrocenylpnictogenium Ions

Corina Stoian,[a] Marian Olaru,[a] Serhiy Demeshko,[b] Malte Fischer,[b] Stefan Mebs,*[c] Emanuel Hupf,*[a] and Jens Beckmann*[a]

The synthesis, characterization and reactivity of the diferrocenylphosphenium ion $[Fc_2P]^+$ was extended to the heavier diferrocenylpnictogenium ions, $[Fc_2E]^+$ (E = As, Sb, Bi). The lighter diferrocenylnitrenium ion, $[Fc_2N]^+$, was detected by mass spectrometry, but could not be isolated. The molecular structures of $[Fc_2E]^+$ (E = P, As, Sb, Bi) reveal intramolecular coordination of the iron atoms, which counterbalance the electron deficiency of the pnictogens without affecting the strong Lewis acidities, which were determined according to the method of Gutmann and Beckett. The (electro−)chemical oxidation and reduction afforded the dications $[Fc_2E]^{2+}$ (E = P (unstable), As) and the neutral dipnictogens Fc_2EEFc_2 (E = P, As).

Introduction

The taming of highly reactive main group cations, coined "cationic beasts" by Krossing *et al.*, poses a substantial challenge that is motivated by potential applications in catalysis and material sciences.[1] Two universal strategies to control the reactivity of electron-deficient species involve the kinetic stabilization with bulky substituents and the electronic stabilization with donor ligands or a combination of both.

The extraordinary stability of ferrocenylcarbenium ions, $[RR'FcC]^+$ (**I**), is attributed to electronic stabilization. The electronic structure has been described as a fulvene-cyclopentadienyl iron cation that engages in through-space interaction with the exocyclic carbon atom (Scheme 1).[2–8] This description is consistent with geometrical parameters found in the molecular structure of $[Ph_2FcC]^+$.[5] The short C–C distance to the exocyclic carbon atom (1.416(9) Å) and the dip angle α[9] (20.7°) suggest a substantial double bond character, while the short intramolecular Fe–C distance (2.715(6) Å) is indicative of an attractive interaction.

Similar trends were observed in the isoelectronic neutral ferrocenylboranes, RR'FcB (**II**), wherein the extent of the distortion from the coplanarity of the boron atom with the Cp ring vastly depends on the Lewis acidity induced by the substituents R and R' (Scheme 1).[10–13] This can be exemplified by comparing $(C_6F_5)_2FcB$[11] with Ph_2FcB.[13] In the more Lewis acidic $(C_6F_5)_2FcB$, the dip angle α[9] (16°) is larger and the Fe–B distance (2.924 Å) is shorter than in the non-fluorinated species Ph_2FcB (13° and 3.009 Å). For the ferrocenylboranes, contributions of a fulvene-cyclopentadienyl resonance structure similar to **II** may also be considered.[11] Very recently, it was demonstrated that the Lewis acidity of neutral ferrocenylboranes, RR'FcB, can be increased upon oxidation of the iron to give cationic ferroceniumboranes, $[RR'FcB]^+$, which are lacking any intramolecular Fe···B interactions.[14]

Silylium ions possess a significantly stronger Lewis acidity than carbenium cations.[15] For a number of ferrocenylsilylium ions $[RR'FcSi]^+$ (**III**) the relative Lewis acidity could be estimated experimentally by their ^{29}Si-NMR chemical shifts.[16,17] However, to the best of our knowledge only one example, namely $[Met\text{-}BuFcSi]^+$, was characterized by X-ray crystallography and shows a dramatic distortion from coplanarity. The dip angle α[9] (44.8°) and the Fe–Si distance (2.492(2) Å) point to the largest intramolecular stabilization amongst all known ferrocenyl-stabilized Lewis acids. Unlike ferrocenylcarbenium ions, $[RR'FcC]^+$ (**II**), there appears to be no fulvene character in the ferrocenylsilylium ions $[RR'FcSi]^+$ (**III**) with the positive charge being formally located at the silicon atoms.

About 40 years ago, Cowley's group reported the diferrocenylphosphenium cation, $[Fc_2P]^+$ (**1P**), which was isolated as $[AlCl_4]^-$ salt at the time.[18,19] Based on ^{31}P NMR and ^{57}Fe Mößbauer spectroscopy, it was concluded that the phosphorus atom is two-coordinate and the iron atoms are in the oxidation state +II. No structural data were available at the time to verify the coordination number of the phosphorus atom. Our interest in kinetically-stabilized pnictogenium ions[20–22] prompted us to reinvestigate and structurally characterize the diferrocenylphosphenium cation, $[Fc_2P]^+$, as a more stable $[B\{3,5\text{-}(CF_3)_2\text{-}C_6H_3\}_4]^-$ salt.[23] Like the dimethylferrocenylsilyl cation, $[Met\text{-}BuFcSi]^+$,[16] the diferrocenylphosphenium cation, $[Fc_2P]^+$ (**1P**), turned out to be a Lewis super acid.[23] The dip angles α[9] (36.5° and 21.8°) and the Fe–P distances (2.613(1) Å and 3.062(1) Å) unambiguously showcased the stabilizing effect of the two ferrocenyl substituents. Unfortunately, severe crystallographic disorder

[a] C. Stoian, M. Olaru, E. Hupf, J. Beckmann
Institut für Anorganische Chemie und Kristallographie, Universität Bremen, Leobener Straße 7, 28359 Bremen, Germany
E-mail: hupf@uni-bremen.de
j.beckmann@uni-bremen.de
[b] S. Demeshko, M. Fischer
Institut für Anorganische Chemie, Georg-August-Universität Göttingen, Tammannstraße 4, 37077 Göttingen, Germany
[c] S. Mebs
Institut für Experimentalphysik, Freie Universität Berlin, Arnimallee 14, 14195 Berlin, Germany
E-mail: stefan.mebs@fu-berlin.de

Supporting information for this article is available on the WWW under https://doi.org/10.1002/chem.202403555

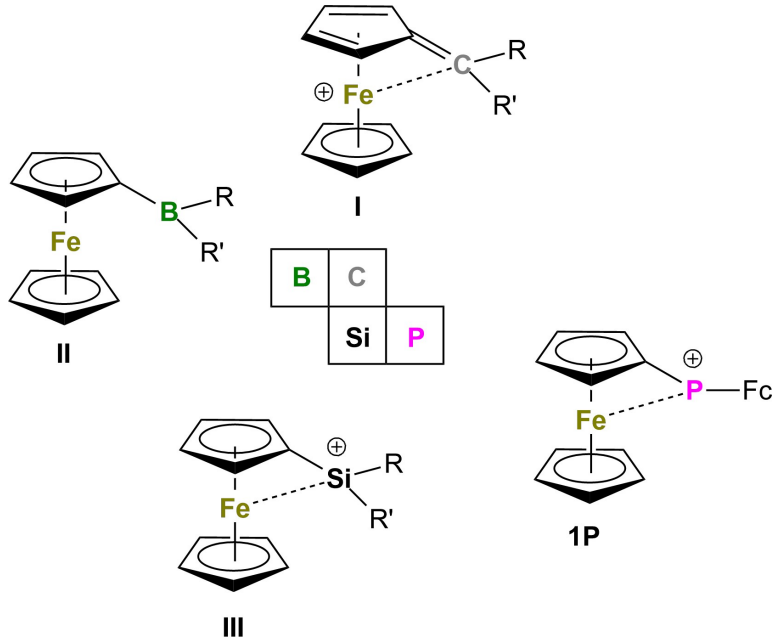

Scheme 1. Ferrocenyl stabilized main group Lewis acids.

precluded the determination of precise P–C bond distances necessary to verify any possible fulvene character of these bonds.[23]

In this work we extended the series of diferrocenylpnictogenium cations, $[Fc_2E]^+$ (**1E**), towards the heavier group 15 elements (E = P, As, Sb, Bi) and isolated the series as $[B(C_6F_5)_4]^-$ salts, which resolved the previous issue with the disorder. We describe our efforts to prepare the related nitrenium ion $[Fc_2N]^+$ (**1N**).[24] The (electro–)chemical reduction and oxidation of **1E** (E = P, As) are also reported. Notably, the diferrocenylpnictogenium cations **1As** and **1Sb** are (quasi) isoelectronic with the germylene Fc^*_2Ge and stannylene Fc^*_2Sn (Fc* = 2,5-bis(3,5-di*t*-butylphenyl)-1-ferrocenyl).[25,26]

Results and Discussion

The reaction of FcLi[27,28] with *i*-Pr_2NECl_2 (E = P,[29] As[30]) and subsequent treatment with a diethyl ether solution of HCl provided the starting materials Fc_2PCl (**2P**)[23] and Fc_2AsCl[31] (**2As**) in 63% and 66% yield, respectively (Scheme 2). Notably, **2P** was previously prepared by a Friedel Crafts type reaction in significantly lower yield of 15%.[32] Alternatively, **2As** was prepared in 86% yield by the reaction FcLi[27,28] with one equivalent of $ZnCl_2$, followed by the addition of half an equivalent of $AsCl_3$. The chloride abstraction of **2P** and **2As** using $K[B(C_6F_5)_4]$[33] gave rise to the phosphenium and the arsenium ions $[Fc_2E][B(C_6F_5)_4]$ (**1E**$[B(C_6F_5)_4]$, E = P, As) in 92% and 86% yield (Scheme 2). The triferrocenylpnictogens Fc_3E (**3E**, E = Sb, Bi) were previously isolated from the reaction of FcLi[27,28] with ECl_3 (Scheme 2).[34,35]

The selective cleavage of one ferrocenyl group from **3Sb** and **3Bi** using $[Ph_3C][B(C_6F_5)_4]$[36] gave rise to the stibenium and the bismuthenium ions $[Fc_2E][B(C_6F_5)_4]$ (**1E**$[B(C_6F_5)_4]$, (E=Sb, Bi) in 78% and 89% yield, respectively (Scheme 2). The by-product, Ph_3CFc,[37,38] was isolated in yields of 92% by washing the reaction mixture with toluene. Alternatively, the stibenium ion **1Sb** was obtained in 84% yield by the protonation of **3Sb** using the pentamethylcyclopentenyl cation $[C_5Me_5H_2][B(C_6F_5)_4]$.[39,40] Efforts to apply the same procedure for **3Bi** gave rise to a complex mixture of products including metallic bismuth and the ferrocenium ion, in which **1Bi** could be detected by NMR spectroscopy. Unfortunately, all our attempts to isolate **1Bi** from this product mixture by fractional crystallization failed. Instead, a few crystals could be isolated, which turned out to be a novel tricyclic pentenyl cation $[C_{10}(CH_2)Me_9H_4][B(C_6F_5)_4]$ that was characterized by X-ray crystallography.[41]

The molecular structures of the pnictogenium ions **1E**$[B(C_6F_5)_4]$ (E = P, As, Sb, Bi) are shown in Figure 1 and selected structural parameters are collected in Table 1. Unlike **1P**$[B\{3,5\text{-}(CF_3)_2\text{-}C_6H_3\}_4]$,[23] the molecular structures of **1E**$[B(C_6F_5)_4]$ (E = P, As, Sb, Bi) are not affected by disorder allowing the unambiguous interpretation of the bond parameters around the

Table 1. Selected bond parameters [Å, °] of **1E**$[B(C_6F_5)_4]$ (E = P, As, Sb, Bi).

	1P	1As	1Sb	1Bi
Fe1–E	2.661(1)	2.744(1)	2.911(1)	2.994(1)
Fe2–E	3.049(1)	3.117(1)	3.168(1)	3.232(1)
E–C10	1.754(4)	1.875(3)	2.078(4)	2.172(5)
E–C30	1.758(4)	1.884(3)	2.068(4)	2.160(5)
C10–E–C30	108.9(2)	106.8(1)	104.2(2)	102.8(2)
α_1[9]	35.6	36.3	36.7	36.1
α_2[9]	19.7	21.6	26.1	26.5

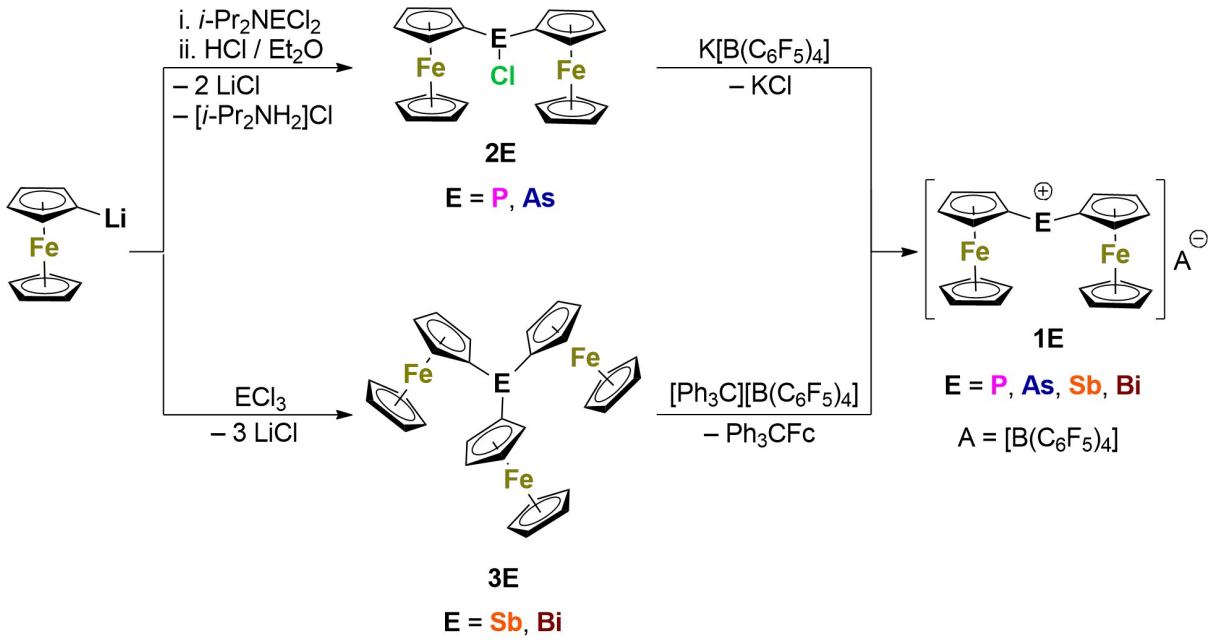

Scheme 2. Synthesis of the diferrocenylpnictogenium ions **1E**[$B(C_6F_5)_4$] (E = P, As, Sb, Bi).

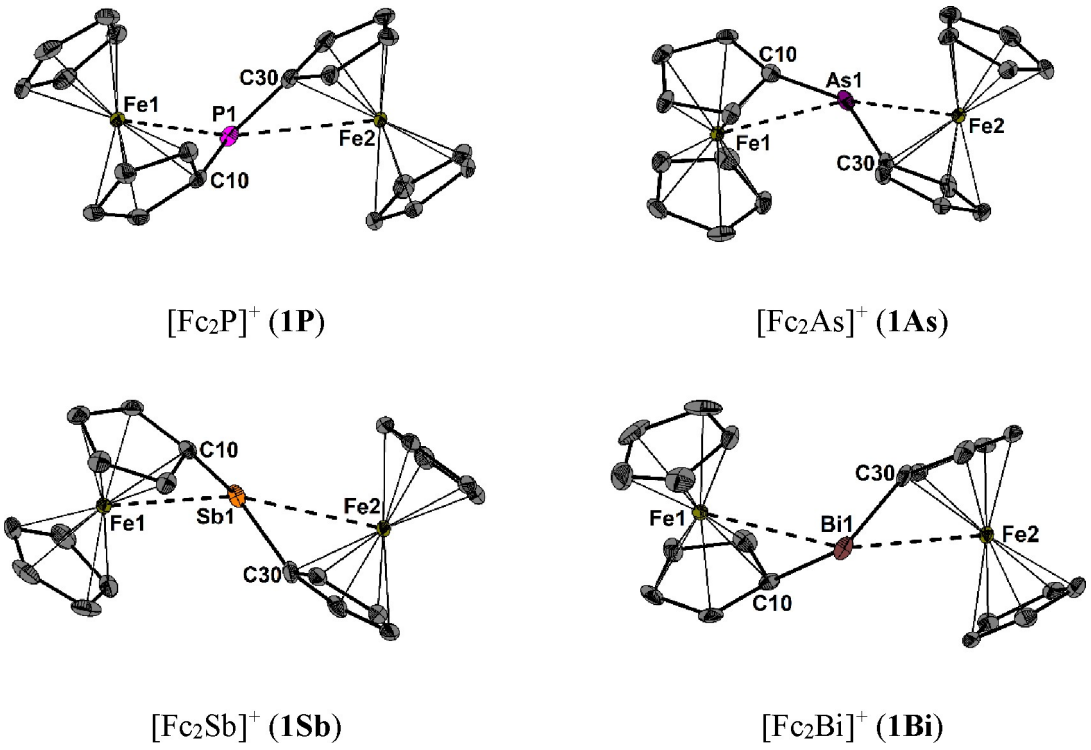

Figure 1. Molecular structures of $[Fc_2E]^+$ (**1E**, E = P, As, Sb, Bi) showing 50% probability ellipsoids and the essential atomic numbering scheme. Hydrogen atoms and $[B(C_6F_5)_4]^-$ counterions are omitted for clarity.

pnictogen atoms. The two crystallographically independent E–C bond lengths (E = P, As, Sb, Bi) are very similar and the P–C bond lengths of **1P**[$B(C_6F_5)_4$] (1.754(4) Å and 1.758(4) Å) are even identical within the experimental error, which rules out that one of the ferrocenyl groups possesses fulvene character.[23] The averaged E–C bond lengths of the two-coordinate **1P** (1.756(4) Å), **1As** (1.880(3) Å), **1Sb** (2.073(4) Å) and **1Bi** (2.166(5) Å) are generally shorter than those of the triferrocenylpnictogens, Fc_3E, **3P** (1.806(8) Å), **3As** (1.961(1) Å), **3Sb** (2.130(2) Å) and **3Bi** (2.227(4) Å).[34] The C–E–C bond angles decrease steadily from **1P** (108.9(2)°) to **1Bi** (102.8(2)°), which can be attributed to the increasing hybridization defect upon descending group

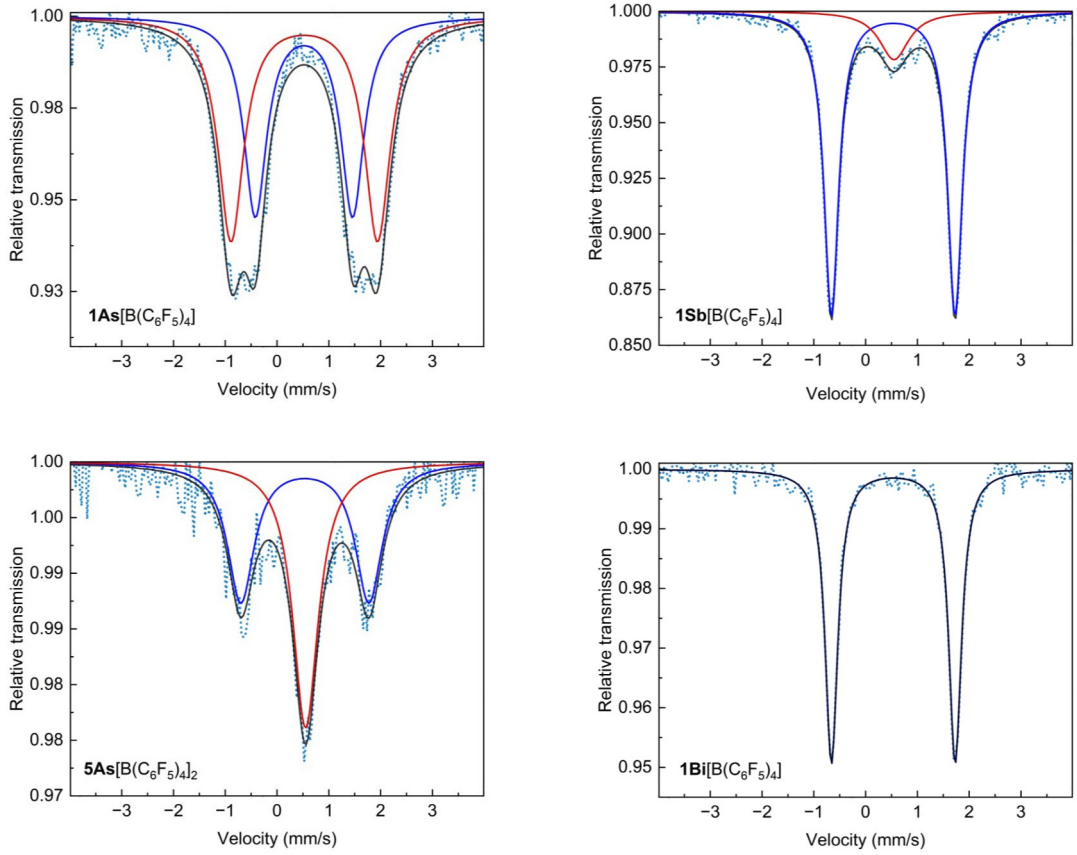

Figure 2. ^{57}Fe Mößbauer spectra of **1E**[B(C_6F_5)$_4$] (E = As, Sb, Bi) and **5As**[B(C_6F_5)$_4$]$_2$, collected in solid state at 80 K. Red and blue lines represent the individual subspectra, the black line is the overall fitting curve.

15.[42] The structures of cations **1E** (E = P–Bi) are asymmetric in that they feature a stronger secondary interaction with the Fe atom of one of the two ferrocenyl groups. The shorter Fe1–E contacts and the longer Fe2–E contacts steadily increase from 2.661(1) Å to 2.994(1) Å and from 3.049(1) Å to 3.232(1) Å, respectively, upon descending group 15 (Table 1). The shorter Fe1–E contacts are associated with dip angles α_1[9] ranging from 35.6° to 36.1°. These values are in between those of [Ph_2FcC]$^+$, (20.7°)[5] and [Me*t*-BuFcSi]$^+$, (44.8°),[16] which approximately correlates with the Lewis acidity (*vide infra*). The second dip angle α_2[9] increases significantly from **1P** (19.7°) and **1As** (21.6°) to **1Sb** (26.1) and **1Bi** (26.5). In contrast, in the less Lewis acidic starting materials Fc_2ECl (**2E**, E = P,[23] As) and Fc_3E (**3E**, E = Sb, Bi)[32] the bonded Cp groups are essentially coplanar with the pnictogen atoms.

In their original communication from 1981, Cowley *et al.* relied on ^{57}Fe Mößbauer spectroscopy to conclude that in **1P**[$AlCl_4$]$^-$ both iron atoms are in the oxidation state +II.[18] It showed a quadrupole doublet with an isomer shift of δ = 0.53 mm s^{-1} and quadrupole splitting of ΔE_Q = 2.33 mm s^{-1} at 60 K, similar to that of ferrocene ((δ = 0.45 mm s^{-1}, ΔE_Q = 2.40 mm s^{-1} at 300 K). In their full paper from 1983, the authors also depictured the Mößbauer spectrum of **1P**, where an unspecified subspectrum with an isomer shift of approx. 0.5 to 0.6 mm s^{-1} can be observed.[19] This signal may indicate a small amount of Fe(III) species, which was, however, not discussed.

The ^{57}Fe Mößbauer spectra for the heavier pnictogenium ions **1As**, **1Sb** and **1Bi** as their [B(C_6F_5)$_4$]$^-$ salts are depicted in the Figure 2 and the related parameters are collected in Table 2. The ^{57}Fe Mößbauer spectrum of **1As** exhibits two quadrupole doublets of approximately equal intensity with very similar isomer shifts of δ_1 = 0.52 mm s^{-1} and δ_2 = 0.53 mm s^{-1} and quite different quadrupolar splitting values of ΔE_{Q1} = 1.88 mm s^{-1} and ΔE_{Q2} = 2.83 mm s^{-1}, which were assigned to the non-equivalent Fe(II) sites. The ^{57}Fe Mößbauer spectra of **1Sb** and **1Bi** show

Table 2. ^{57}Fe Mößbauer parameters of **1E**[B(C_6F_5)$_4$] (E = P, As, Sb, Bi) and **5As**[B(C_6F_5)$_4$]$_2$ collected in the solid state at 80 K.

	δ_1 (mm s^{-1})	ΔE_{Q1} (mm s^{-1})	δ_2 (mm s^{-1})	ΔE_{Q2} (mm s^{-1})	I_{rel1} (%)	I_{rel2} (%)
1P[18]	0.53	2.33	0.57	–	–	–
1As	0.52	1.88	0.53	2.83	44.3	55.7
1Sb	0.53	2.39	0.55	0.05	86.3	13.7
1Bi	0.53	2.39	–	–	100.0	–
5As	0.54	2.47	0.55	0.04	52.1	47.9

only one quadrupole doublet for the two Fe(II) sites with identical values at $\delta_1 = 0.53\ mm\,s^{-1}$ and $\Delta E_{Q1} = 2.39\ mm\,s^{-1}$. Similar to **1P**,[19] the ^{57}Fe Mößbauer spectrum of an otherwise freshly isolated sample of **1Sb** reveals a second non-resolved subspectrum at $\delta_2 = 0.55\ mm\,s^{-1}$ and $\Delta E_{Q1} = 0.05\ mm\,s^{-1}$ with a relative intensity of 13.7%, which was assigned to an Fe(III) site of unknown origin.

The calculated gas-phase structures of **1P**–**1Bi** are almost symmetrical despite being optimized without symmetry restrictions. Deviations from symmetry compared to the experimental structures apparently stem from crystal packing effects (Table 1 and Table S6). The calculated E–C bond lengths increase from ca. 1.753 Å to 2.171 Å, whereas the E–Fe distances increase from 2.780/2.787 Å to 3.084/3.085 Å (Table S6). The bonding situation of the pnictogen (E) atoms was analyzed using a set of real-space bonding indicators (RSBI), including topological bond paths analysis using the atoms in molecules (AIM)[43] approach, investigation of weak secondary interactions by the non-covalent interactions (NCI)[44] index, as well as the electron localizability indicator (ELI–D),[45] complementing AIM.[46] Since the AIM analysis using the electron density (ED) typically fails to reliably display bond types with flat ED gradients, the more stable virial field (VF) function was used instead.[46] As was found previously for **1P**,[23] all primary E–C, C–C, and C–H bonds and most Fe–C bonds cause the formation of a virial path, whereas no E···Fe paths are formed for **1P** up to **1Bi**, leaving this type of interaction to be largely non-covalent. This is supported by the NCI *iso*-surfaces, which shows ring-shaped and red-colored basins for each CpFe interaction, revealing their largely covalent nature, but localized blueish-colored basins along the E···Fe and adjacent E···H axes, indicating weak and purely non-covalent atom-atom contacts (Figures S66 and S67).[46,47] The bonding characteristics of the primary E–C interactions are polar-covalent for all four compounds, with dominating covalent bonding aspects in the P–C bond whereas largely diminishing relevance of covalence are observed in the Bi–C bond.[47]

The diferrocenylpnictogenium ions **1E** (E = P, As, Sb, Bi) reveal intense colors in solution (Figure 3). The UV-vis absorption spectra of the pnictogenium ions show large bands in the visible region with stronger absorption maxima between λ_{max} = 504–516 nm for **1E** (E = P, As, Sb). A noticeable difference is present in the spectrum of **1Bi**, with a bathochromically shifted absorption maximum (λ_{max} = 548 nm) in comparison to the lighter analogues. Time-dependent DFT (TD-DFT) was subsequently conducted for **1E** (E = P, As, Sb, Bi) to obtain theoretical UV-vis spectra (Figure S68 and Tables S7–S10). All four spectra deviate from the experimentally obtained ones with the main strong transitions at λ_{max} = 440 (**1P**), 438 (**1As**), 436 (**1Sb**), and 440 (**1Bi**) nm, which can be assigned to multiple orbital transitions with comparable contributions. The asymmetric shape of the calculated UV-vis spectra (shoulder on the right side) is mainly caused by a transition at λ_{max} = 480 nm (**1P**), 480 nm (**1As**), 478 nm (**1Sb**), and 480 nm (**1Bi**). The frontier orbital energies of **1E** are shown in Figure S69 and Table S11. Along the series **1P** to **1Bi**, the HOMO, HOMO(−n), and LUMO (+n; n = 1–4) steadily increase, whereas the LUMO rather follows a zigzag progression, resulting in band gaps E_{gap} of

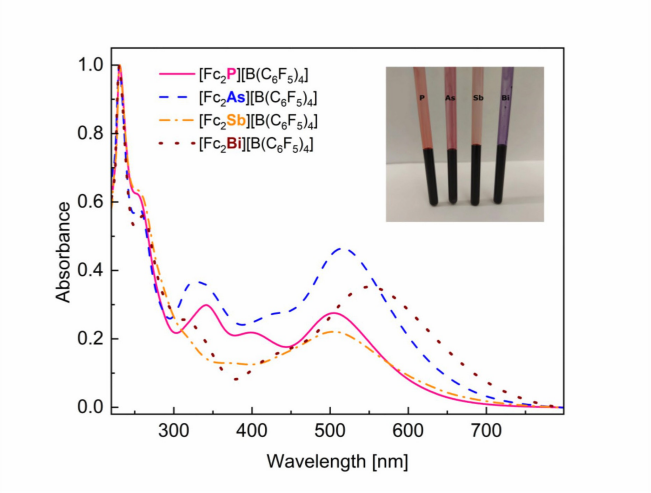

Figure 3. Normalized UV-vis absorption spectra and absorption maxima of **1E**[$B(C_6F_5)_4$] (E = P (pink), λ_{max} = 504.4, 398.5, 341.3 nm; E = As (blue) λ_{max} = 515.9, 327.1 nm; E = Sb (yellow) λ_{max} = 503.8 nm; E = Bi (dark red) λ_{max} = 548.1 nm).

0.140 (**1P**), 0.136 (**1As**), 0.139 (**1Sb**), and 0.134 (**1Bi**) a.u., explaining the overall similar color of the four species. As observed for **1P**,[23] the HOMOs of the heavier analogues are clearly dominated by Fe(d) contributions, with little involvement of P(s,p_x,p_y), and C(s,p) orbitals, together accounting for the Fe–C and P–C interactions (Figures S70 and S71). In contrast, the LUMO is generated by the empty p_z orbital of the pnictogen atom in conjunction with some Fe(d_z^2) and minor C(p) aspects of the carbon atom close to the pnictogen atom, whereas higher LUMOs are solely characterized by antibonding Fe–C contributions and no involvement of the pnictogen atom.

The Lewis acidic diferrocenylphosphenium ion **1P** undergoes complex formation with Lewis bases, such as *n*-Bu_3P,[18,19] Ph_3P and 1,3-bis(2,6-di-*i*-propylphenyl)imidazole-2-ylidene (IPr).[23] In CD_2Cl_2, the ^{31}P NMR chemical shift of **1P** (δ = 183.5 ppm) is indicative for the deshielded phosphorus atom.[18,19] Interestingly, this value does not change upon addition of THF or MeCN, which suggests that these solvents do not coordinate to **1P**. In contrast, the addition of pyridine and tetrahydrothiophene (tht) results in a shift of the ^{31}P NMR resonance (to 113.9 ppm and to 119.8 ppm), which is indicative for the formation of donor acceptor complexes in solution. Addition of Et_3N or quinoline, as well as THF or MeCN (after 2 days), induce decomposition. The Lewis acidity of the cations **1E** (E = P, As, Sb, Bi) was quantitatively assessed using Gutmann-Beckett acceptor numbers, which are based upon ^{31}P NMR chemical shift differences of the reversible coordination of Et_3PO (in CD_2Cl_2).[48,49] The acceptor numbers indicate that the Lewis acidity decreases in order of the atomic number from 117 (**1P**), 96 (**1As**), 92 (**1Sb**) to 75 (**1Bi**). The same trend was also found for the kinetically stabilized phosphenium ions, M^SFluindMesE$^+$, however, the acceptor numbers of 132 (**1P**), 116 (**1As**), 101 (**1Sb**) and 23 (**1Bi**, value for $CDCl_3$) are higher for the lighter elements, but decline more intensely descending group 15.[21,22] In fact, the bismuthenium ion M^SFluindMesBi$^+$

shows no reactivity as Lewis acid towards Et_3PO, presumably due to the limited space in the congested environment of the M^{S}Fluind substituent. The calculated fluoride ion affinity (FIA) is used as an estimate for the strength of the isolated Lewis acids. For **1E** (E = P, As, Sb, Bi) it spans a range from 660 to 621, confirming the experimentally observed trend (Table S12). The calculated fluoride ion affinity (FIA)[50] values are in between the kinetically-stabilized bis(*m*-terphenyl)pnictogenium ions [2,6-$Mes_2C_6H_3)_2E]^+$ (701 to 602) and the M^{S}Fluind-substituted pnictogenium ions [M^{S}FluindMesE]$^+$ (M^{S}Fluind = dispiro[fluorene-9,3′-(1′,1′,7′,7′-tetramethyls-hydrindacen-4′-yl)-5′,9′′-fluorene; 639 to 559).[22] All of these values lie above the defined Lewis superacidity threshold for SbF_5 (443 to 508 against Me_3Si^+/Me_3SiF and depending on the level of theory).[50]

Attempted Preparation of the Nitrenium Ion $[Fc_2N][B(C_6F_5)_4]$ (1N)

In 1999, Bildstein *et al.* described a failed attempt to prepare the nitrenium ion $[Fc_2N][BF_4]$ by the reaction of Fc_2NH with $[Ph_3C][BF_4]$.[24] In an effort to complete the series of diferrocenylpnictogenium ions, $[Fc_2E]^+$ (**1E**, E = P, As, Sb, Bi), and encouraged by the successful synthesis of the related dicobaltocenium amide $[Cc_2N][PF_6]$, recently reported by Förster and Heinze *et al.*,[51] we reinvestigated the same reaction, but replaced the labile $[BF_4]^-$ counterion with the more robust $[B(C_6F_5)_4]^-$. The reaction of Fc_2NH with $[Ph_3C][B(C_6F_5)_4]$ afforded a dark reaction mixture, similar to that reported by Bildstein *et al.*[24] However, ^{1}H- and ^{13}C-NMR spectra of the reaction mixture exhibited only very broad signals. The speciation of cationic products in the reaction mixture by electrospray mass spectrometry revealed a prominent mass cluster at m/z = 384 Da that was tentatively assigned to $[Fc_2N]^+$ (**1 N**, Figure 4). The mass spectrum showed another overlapping mass cluster at m/z = 385 Da that was assigned to $[Fc_2NH]^+$, which might have formed by a single electron transfer (SET) and can be either a mixed-valent (Fe(II/III)) secondary amine or an aminium radical cation. This observation is consistent with the most recent attempts to generate nitrenium ions in the literature.[52,53] The same mass spectrum also comprised higher mass clusters at m/z = 627 Da and 869 Da that were assigned to $[Fc_2N(CPh_3)_n]^+$ (n = 1, 2), which, again, can be either assigned to a mixed-valent (Fe(II/III)) tertiary amine, an aminium radical cation or the quaternary ammonium ion $[Fc_2N(CPh_3)_2]^+$ (Figure 4).

Redox Chemistry of the Pnictogenium Ions $[Fc_2E][B(C_6F_5)_4]$ (1E, E = P, As, Sb, Bi)

The presence of the redox-active ferrocenyl groups in the low valent pnictogenium ions **1E** (E = P, As, Sb, Bi) prompted us to investigate their redox properties. The chemical single-electron reduction of **1P** and **1As** with one equivalent of cobaltocene Cp_2Co gave rise to an immediate color change from dark red to light orange. From the reaction mixture, the diphosphine Fc_2PPFc_2 (**4P**) and the diarsine $Fc_2AsAsFc_2$ (**4As**) were separated from the $[Cp_2Co][B(C_6F_5)_4]$[54] by washing the mixture with acetonitrile and obtained as air-stable crystalline solids in 90 and 95% yield (Scheme 3). We note that **4P** was previously prepared by Cowley by the reduction of Fc_2PCl (**2P**) with Mg turnings or sodium naphthalenide.[19,55] All efforts to reduce **1Sb** and **1Bi** with Cp_2Co resulted in deposition of metallic antimony and bismuth. The molecular structures of **4P** and **4As** are shown in Figure 5. They adopt synperiplanar conformations, similar to that observed for *t*-Bu_2PP*t*-Bu_2,[56] whereas Ph_2PPPh_2[57] and $Ph_2AsAsPh_2$[58] possess antiperiplanar conformations. The related C–E–E–C torsion angles (E = P, As) of **4P** (4.9 °), **4As** (−2.0 °) are smaller than that of *t*-Bu_2PP*t*-Bu_2 (12.3 °)[56] and the E–E bond lengths (E = P, As) of **4P** (2.258(1) Å) and **4As** (2.480(1) Å) are slightly longer than those of Ph_2PPPh_2 (2.217(2) Å)[57] and $Ph_2AsAsPh_2$ (2.460(1) Å).[58] The chemical single-electron oxidation of **4P** and **4As** with varying equivalents of the silver tetrakis(pentafluorophenyl)borate benzene solvate $[Ag(C_6H_6)_3][B(C_6F_5)_4]$[59] was monitored by ^{31}P and ^{1}H NMR spectroscopy.[60] The addition of one equivalent of the silver salt resulted in the cleavage of the E–E bonds (E=P, As) and formation of unidentified silver compounds along with the

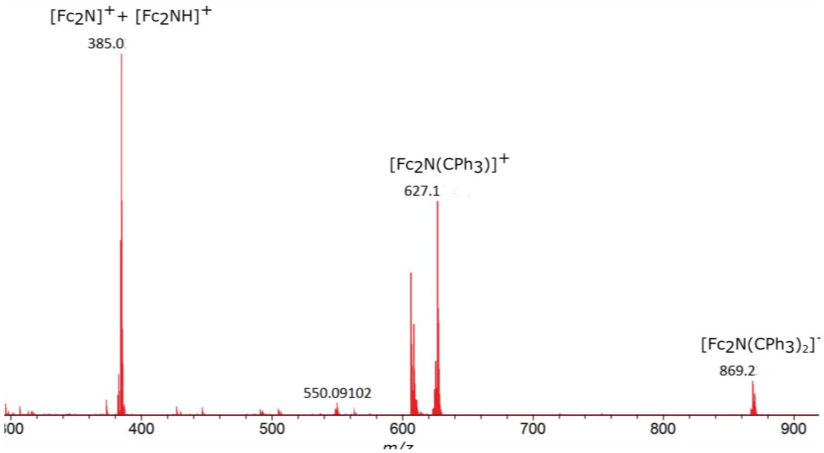

Figure 4. Electrospray mass spectrum (CH_2Cl_2, positive mode) of reaction mixture of Fc_2NH with $[Ph_3C][B(C_6F_5)_4]$.

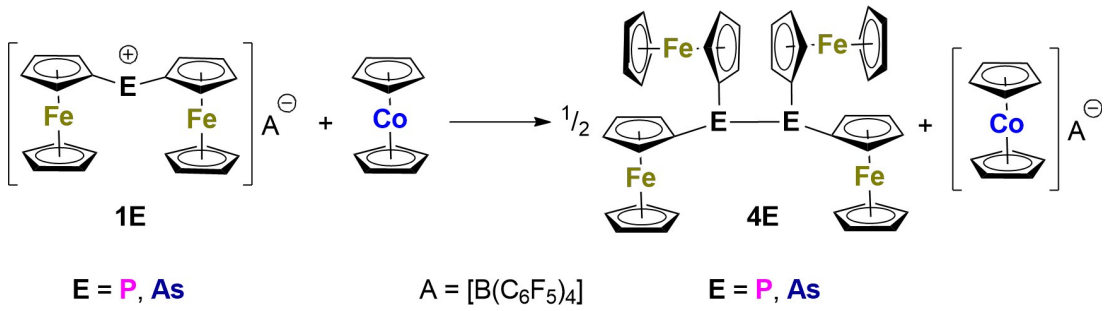

Scheme 3. Reduction of the pnictogenium ions $[Fc_2E][B(C_6F_5)_4]$ (**1E**, E = P, As).

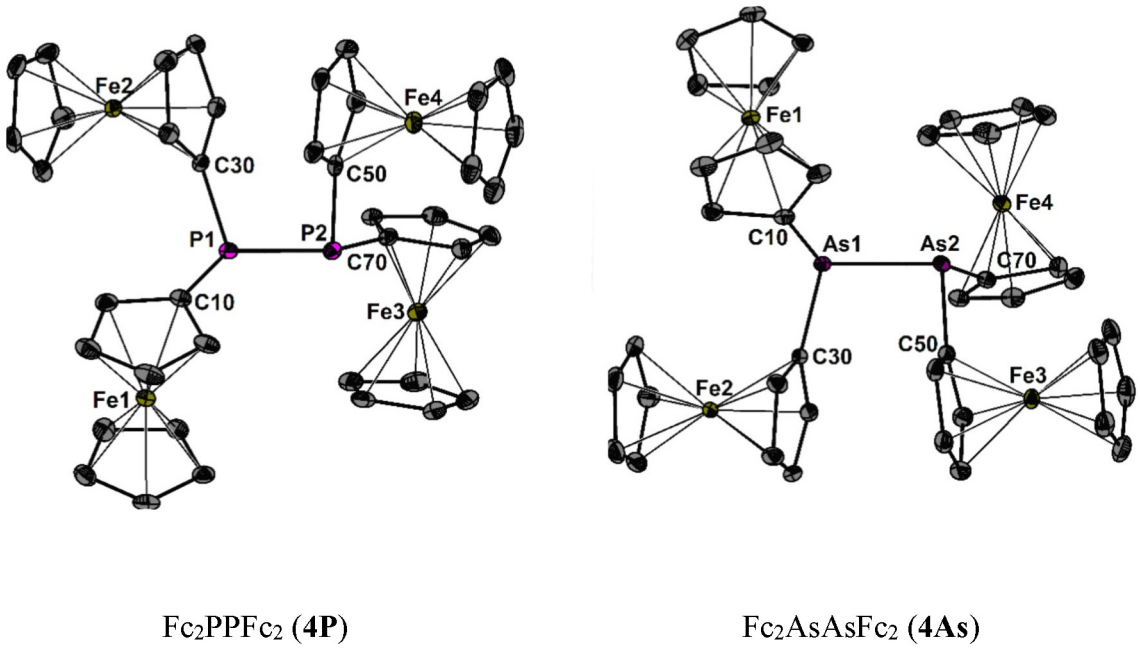

Fc_2PPFc_2 (**4P**) $Fc_2AsAsFc_2$ (**4As**)

Figure 5. Molecular structures of Fc_2EEFc_2 (**4E**, E = P, As) showing 50% probability ellipsoids and the essential atomic numbering scheme. Hydrogen atoms are omitted for clarity.

corresponding cations **1P** and **1As**, while with two equivalents of the silver salt the reaction proceeded to the quantitative (reverse) formation of **1P** and **1As** (Scheme 4). This result is in sharp contrast to the observations made by Wang *et al.* who studied the stepwise single-electron oxidation of a bulky tetraaryldiposphines, R_2PPR_2, with silver salts yielding a radical cation $[R_2PPR_2]^{\bullet+}$ and a related dication $[R_2PPR_2]^{2+}$ (R = 2,4,6-*i*-$Pr_3C_6H_3$) without affecting the integrity of the P–P bond.[61,62] The chemical single-electron oxidation of **1P** and **1As** with one equivalent of $[Ag(C_6H_6)_3][B(C_6F_5)_4]$ was accompanied by a rapid

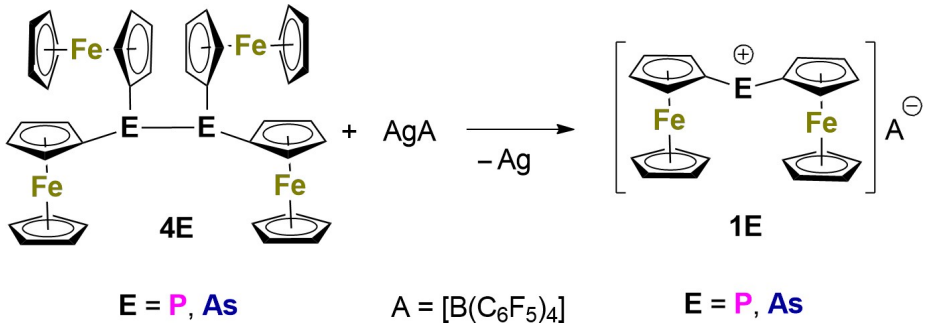

Scheme 4. Oxidation of Fc_2EEFc_2 (**4E**, E = P, As).

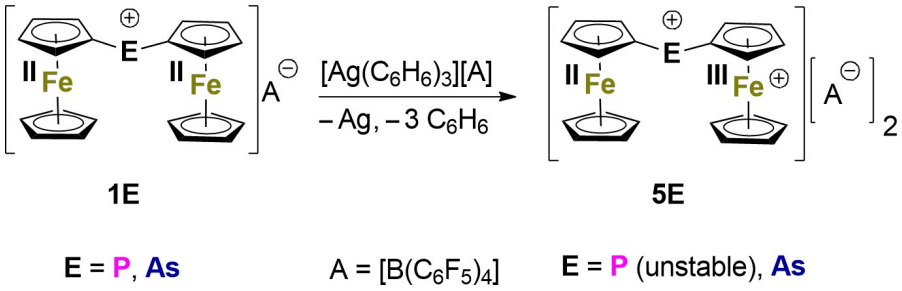

Scheme 5. Oxidation of $[Fc_2E][B(C_6F_5)_4]$ (**1E**, E = P, As).

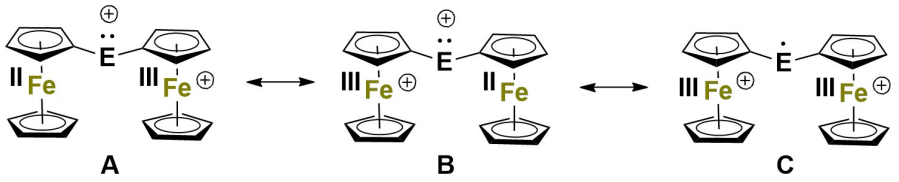

Scheme 6. Possible resonance structures of $[Fc_2E]^{2+}$ (**5E**, E = P, As).

change in color from dark red to dark brown (**1P**) and to dark green (**1As**), respectively, and afforded the corresponding mixed-valent dications $[Fc_2E]^{2+}$ (**5E**, E=P, As) in solution (Scheme 5). All attempts to grow single crystals of **5P** and **5As** suitable for X-ray diffraction analysis failed, but **5As**$[B(C_6F_5)_4]_2$ was isolated as NMR and EPR silent solid in 89% yield.

Unlike the mixed valent $[Fc_3E]^+$ (E = As, Sb, Bi),[32] UV-vis spectrum of **5As** does not show intervalence charge-transfer bands, but exhibits absorption maxima at 498 nm and 628 nm (Figure 6).

The ^{57}Fe Mößbauer spectrum of **5As** reveals a doublet with an isomer shift of $\delta_1 = 0.54$ mm s^{-1} and a quadrupole splitting of $\Delta E_{Q1} = 2.47$ mm s^{-1} for the Fe(II) sites and a non-resolved doublet with an isomer shift of $\delta_2 = 0.55$ mm s^{-1} and a quadrupole splitting of $\Delta E_{Q1} = 0.04$ mm s^{-1} for the Fe(III) sites (Figure 2, Table 2). Thus, the Mößbauer data of **5As** suggest that the electronic situation is best described by mixed-valent resonance structures **A** and **B** (Scheme 6). The ^{31}P NMR spectrum (CD_2Cl_2) of a freshly prepared sample of **5P** exhibits a very broad singlet resonance signal at $\delta = 221$ ppm ($\omega_{1/2} = 1228$ Hz),[63] which is more deshielded than the sharp signal of **1P** ($\delta = 183.5$ ppm).[23] In solution, **5P** rapidly undergoes decomposition to give other phosphorus-containing species, which was followed by ^{31}P, ^{19}F NMR and ^{57}Fe Mößbauer spectroscopy.[64]

Compared to the pnictogenium cations $[Fc_2E]^+$ (**1E**), the calculated structures of the pnictogenium dications, $[Fc_2E]^{2+}$ **5E** (E = P, As, Sb, Bi), are characterized by slightly increased E–C bond lengths (P–C 1.793 Å, Δ = 0.040 Å; As–C 1.923 Å, Δ = 0.047 Å; Sb–C 2.139 Å, Δ −0.063 Å; Bi–C 2.245 Å, Δ = 0.073 Å) as well as well as by significantly longer Fe···E distances (P–Fe 3.366 Å, Δ = 0.581 Å; As–Fe 3.486 Å, Δ = 0.618 Å; Sb–Fe 3.714 Å, Δ = 0.712 Å; Bi–Fe 3.840 Å, Δ = 0.755 Å), which excludes the existence of stabilizing E···Fe interactions similarly as in **1E**. The C–E–C angles decreased to 102.17° (**5P**), 98.91° (**5As**), 94.57° (**5Sb**), and 92.60 (**5Bi**). The AIM virial field analyses of **5E** (E = P, As, Sb, Bi) lacks any intramolecular contacts (Figure S72). The AIM charges **5E** of the pnictogen atoms are 1.24 e (**5P**), 0.80 e

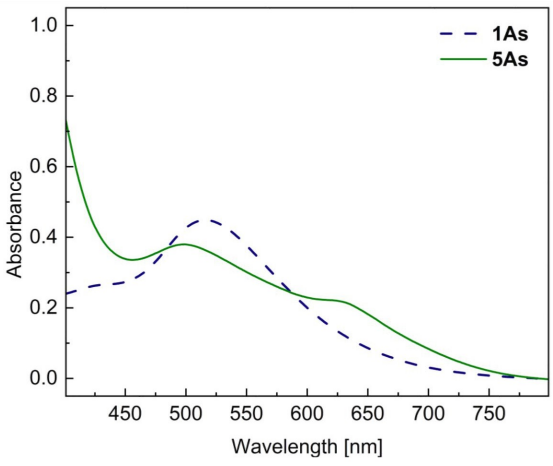

Figure 6. Normalized UV-vis absorption spectra of **1As** (blue) and **5As** (green).

Table 3. Electrochemical data for **1E** (E = P, As, Sb, Bi), **4P** and **4As** at 100 mVs^{-1} scan rate (0.5 mM, CH_2Cl_2, [*n*-Bu_4N][$B(C_6F_5)_4$], E *vs* Fc/Fc^+ redox couple).

Compound	E_{pa1} (mV)	E_{pa2} (mV)	E_{pa3} (mV)	E_{pa4} (mV)	E_{pa5} (mV)
1P	−490	+104	–	–	–
1As	−651	−384	−106	−35	–
1Sb	−612	−358	–	–	–
1Bi	−580	−326	−236	+118	–
4P	−52	+223	+428	+521	+738
4As	−99	+172	+477	+699	–

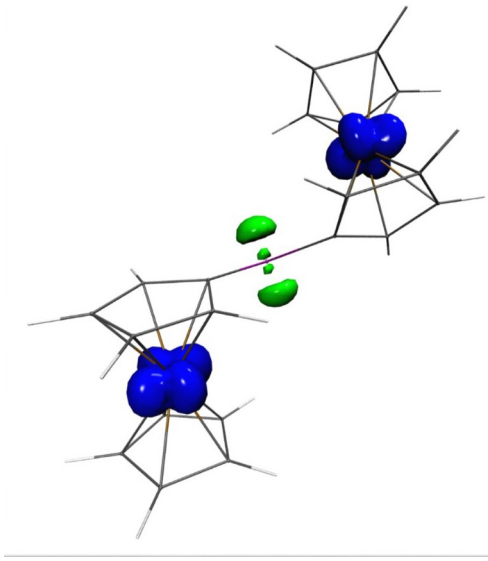

Figure 7. Spin density of **5As**, representation at +/−0.02 a.u. (blue/green).

(**5As**), 0.94 e (**5Sb**), and 0.89 e (**5Bi**), which are surprisingly less positive compared to those of **1E** (Δ = 0.19 e, 0.15 e, 0.21 e, and 0.20 e). Nevertheless, the FIA-values of the dications **5E** (E = P, 997; E = As, 887) are significantly larger than those of the monocations **1E** (E = P, 660; E = As, 635). The Mulliken spin densities **5E** are calculated to be similar for all four dicationic compounds, ranging from −0.24 to −0.30 e for the pnictogen atom and from 0.90 to 0.96 e for the Fe atoms (Figures 7 and S73). Thus, the results obtained from the DFT calculations are somewhat contradictory to the Mößbauer data of **5As**, which favor the mixed-valent resonance structures **A** and **B** (Scheme 6). The lack of intramolecular Fe···E interactions, the distribution of spin densities over the iron and pnictogen atoms as well as the reduced AIM charges at the pnictogenes suggest that the resonance structure **C** featuring two iron(III) sites and open-shell pnictogens may play a certain role (Scheme 6). To resolve this apparent contradiction calls for more in-depth (multi-reference) calculations, which are beyond the scope of this work.

The cyclic voltammograms of the monocations **1E** (E = P, As, Sb and Bi) as well as those of **4P** and **4As** were recorded in anhydrous and degassed solutions of [*n*-Bu_4N][$B(C_6F_5)_4$] (25 mM) in dichloromethane at 25 °C, and under argon atmosphere, due to high reactivity of the cations. The supporting electrolyte contains the weakly coordinated anion, which is also known to stabilize highly charged species in solution and increases redox splitting.[65] The corresponding voltammograms are shown in Figure 8, while the oxidation potentials *vs* the Fc/Fc^+ redox couple are summarized in Table 3. The pnictogenium ions **1P**, **1Sb** and **1Bi** show multiple, partially overlapping, redox events, with the first oxidation events being quasi-reversible. On the other hand, **1As** shows four redox processes, where the first oxidation is irreversible. Given the nature of these cations, it is possible that the follow-on reactions during the measurements would be a consequence of high sensitivity to air and moisture.

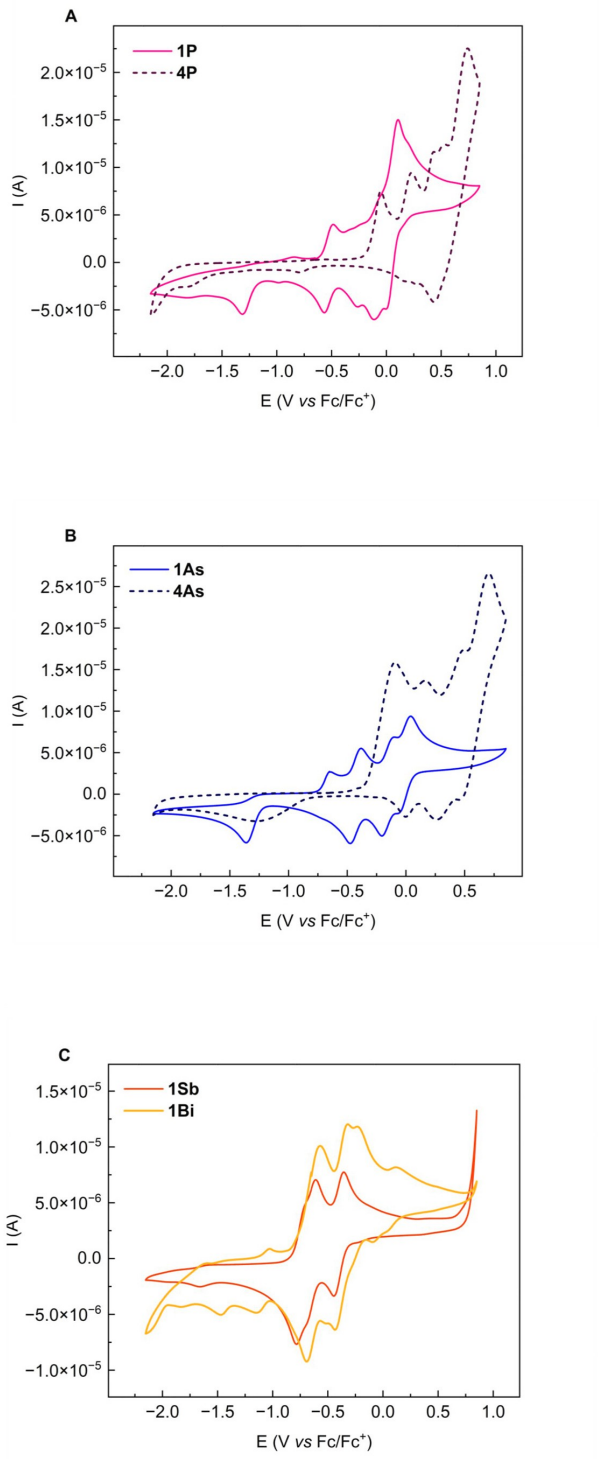

Figure 8. Cyclic voltammograms (0.5 mM, CH_2Cl_2, [*n*-Bu_4N][$B(C_6F_5)_4$]) of A) **1P** and **4P**, B) **1As** and **4As**, C) **1Sb** and **1Bi**, potential sweep rate 50 mV s^{-1}. Plotting convention: IUPAC (direction of the scan: toward positive potentials (to the right); initial potential: −0.1 V).

Interestingly, the first redox events for the cations **1E** (E = P, As, Sb and Bi) arise at negative potentials, with E_{pa1} for **1As** as low as −651 mV (*vs* Fc/Fc^+). Notably, compounds **4P** and **4As** show five and four redox events respectively, with large peak-to-peak

separation. In both cases, the first oxidation is irreversible and appears to follow an 'ECE' like mechanism. The redox processes for **4P** shift to more positive potentials compared to **4As** (Table 3), although the first oxidation potential is comparable to the one of **3P** and **3As** ($E_{pa1} = -50$ mV *vs* Fc/Fc^+).[34]

Conclusions

Synthetic protocols for the preparation of an almost complete series of diferrocenylpnictogenium ions, $[Fc_2E]^+$ (**1E**, E=P, As, Sb, Bi) were developed. Only the synthesis of the lightest member of the compound class, namely, the nitrenium ion $[Fc_2N]^+$ (**1 N**) was deemed impossible, although a related mass cluster was detected by mass spectrometry. Unlike previously assumed for the diferrocenylphosphenium ion, $[Fc_2P]^+$ (**1P**), the pnictogens in $[Fc_2E]^+$ (**1E**, E = As, Sb, Bi) are not strictly two-coordinated,[23] but intramolecularly coordinated by the iron atoms of the ferrocenyl groups. This intramolecular coordination moderates the putative Lewis acidity only marginally. The (electro−)chemical oxidation and reduction afforded the dications $[Fc_2E]^{2+}$ (E = P (unstable), As) and the neutral dipnictogens Fc_2EEFc_2 (E = P, As) having unprecedently labile E–E bonds. The chemical oxidation of the latter affords the monocations $[Fc_2E]^+$ (**1E**, E = P, As). Efforts are underway to use diferrocenylpnictogenium ions for the activation of small molecules.

Experimental Section

General Information

Unless otherwise stated, all the reactions, manipulations work-up and purifications were performed under inert argon atmosphere using anhydrous solvents. The reagents used in this work including ferrocene and *n*-BuLi were obtained commercially and used as received. Fc_2PCl,[23] Fc_2PH,[19] FcLi,[27,28] *i*-Pr_2NAsCl_2,[30] Fc_2NH,[66] Fc_3Sb, Fc_3Bi,[34,35] $K[B(C_6F_5)_4]$,[33] $[C_5Me_5H_2][B(C_6F_5)_4]$,[40] cobaltocene,[67,68] [*n*-$Bu_4N][B(C_6F_5)_4]$,[65] and $Ag(C_6H_6)_3[B(C_6F_5)_4]$,[59] were prepared following the procedures described in the literature. Anhydrous dichloromethane, tetrahydrofuran, *n*-hexane, acetonitrile, and toluene were collected from an SPS800 mBraun solvent purification system and stored over 3 Å molecular sieves. Diethyl ether was dried by heating at reflux over Na/benzophenone under argon atmosphere. Deuterated solvents were degassed and dried over 3 Å molecular sieves under argon. Other solvents, such as 1,2-difluorobeneze or 3-fluorotoluene, were dried directly over 3 Å molecular sieves.

Unless otherwise noted, NMR spectra were recorded at room temperature on a Bruker Avance Neo 600 MHz spectrometer. ^1H, $^{13}C\{^1H\}$, ^{11}B, ^{19}F, and ^{31}P NMR spectra are reported on the δ scale (ppm) and are referenced against $SiMe_4$, $BF_3{\cdot}Et_2O$ (15% in $CDCl_3$), $CFCl_3$, and H_3PO_4 (85% in water) respectively. ^1H and $^{13}C\{^1H\}$ chemical shifts are referenced to the residual peak of the solvent ($CDHCl_2$ 5.32 ppm for CD_2Cl_2) in the ^1H NMR spectra, and to the peak of the deuterated solvent (CD_2Cl_2 53.84 ppm) in the $^{13}C\{^1H\}$ NMR spectra.[69]

The ESI HRMS spectra were measured on a Bruker Impact II spectrometer. Dichloromethane, acetonitrile, or dichloromethane/acetonitrile solutions ($c = 1{\cdot}10^{-5}$ mol L^{-1}) were injected directly into the spectrometer at a flow rate of 3 μL min^{-1}. Nitrogen was used both as a drying gas and for nebulization with flow rates of approximately 5 L min^{-1} and a pressure of 5 psi. Pressure in the mass analyzer region was usually about $1{\cdot}10^{-5}$ mbar. Spectra were collected for 1 min and averaged. The nozzle-skimmer voltage was adjusted individually for each measurement.

UV-Vis absorption spectra were recorded on a VWR UV-1600PC spectrophotometer, and anylised using Spectragryph software.[70] Melting points were determined on a SCHORPP Gerätetechnik MPM–H3, using one end closed capillary tubes, the other end was closed with silicon grease.

Cyclic voltammetry studies were performed using Microcell Passive setup from *rhd instruments GmbH & Co.KG* combined with the TSC1600 closed measuring cell. The CV data was recorded at room temperature using an Autolab PGSTAT 101 Metrohm potentiostat. A three-electrode configuration was used with a glassy carbon (D = 3 mm) acting as a working electrode (WE), a Pt crucible acting as counter electrode (CE) and an Ag pseudo reference electrode (pRE). Before every measurement, all electrodes were polished to a mirror-like appearance with diamond paste (1 μm) and carefully rinsed with deionized water and HPLC grade acetone. The ferrocene/ferrocenium redox couple (Fc/Fc^+, c = 0.5 mM) was used as an external standard. The cations were measured as 0.5 mM solutions in CH_2Cl_2 prepared in a glovebox. [*n*-$Bu_4N][B(C_6F_5)_4]$ (25 mM) was used as supporting electrolyte.

Mößbauer spectra were recorded with a ^{57}Co source in a Rh matrix using an alternating constant acceleration Wissel Mößbauer spectrometer operated in the transmission mode and equipped with a *Janis* closed-cycle helium cryostat. Isomer shifts were referenced to α-Fe foil at room temperature. Simulation of the experimental data was performed with the *mf2.SL* program using *Lorentzian* line doublets.[69] Electron paramagnetic resonance (EPR) studies were performed on a MiniScope MS400 table-top X-band spectrometer from Magnettech at 138 K (neat solid).

Synthesis of Fc_2AsCl (2As). *Method A:* To a pre-cooled (−80 °C) suspension of FcLi (830 mg, 4.10 mmol, 5% ferrocene) in THF (20 mL), *i*-Pr_2NAsCl_2 (501 mg, 2.02 mmol) was added dropwise. The reaction mixture was allowed to warm up to room temperature over the course of 3 h. A solution of HCl in Et_2O (1.5 M, 1.8 mL, 2.7 mmol) was added slowly at 0 °C and stirred for 30 min at room temperature. The suspension was filtered, and the solvents were evaporated to dryness. CH_2Cl_2 (25 mL) was added, and the suspension was filtered to remove LiCl. The solvent was evaporated to dryness and the remaining orange solid was washed with MeCN (4×4 mL). The remaining solid was dried under vacuum. The product 2As was obtained as an orange solid (640 mg, 66%).

Method B: To a pre-cooled (−80 °C) suspension of FcLi (1.35 g, 7.10 mmol) in THF (20 mL), $ZnCl_2$ (960 mg, 7.04 mmol) was added as a solid. The yellow suspension was allowed to warm up to −20 °C over a course of 2 h, then it was stirred for 30 more min at room temperature. The newly formed FcZnCl solution was cooled down to −80 °C, and $AsCl_3$ (412 mg, 2.27 mmol) was added dropwise. The reaction mixture was stirred overnight. The solvent was evaporated to dryness, then the dark green solid was washed with MeCN (5×5 mL) until the washings were colorless. The orange solid was dried, then washed with 5 mL hexane. The product **2As** was dried under vacuum and was obtained in 86% yield (1.38 g).

M.p. = 160–161 °C (decomp.). **^1H NMR (600 MHz, CD_2Cl_2)**: δ = 4.50 (m, br, 4H, AsCp Hβ),4.41 (m, br, 2H, AsCp Hα), 4.24 (m, br, 2H, AsCp Hα), 4.22 (s, 10H, Cp). **$^{13}C\{^1H\}$ NMR (151 MHz, CD_2Cl_2)**: δ = 81.2 (s, As–Cp *i*-C), 72.7 (s, AsCp Cα), 72.4 (s, AsCp Cβ), 72.2 (s, AsCp Cβ), 71.5 (s, AsCp Cα), 69.6 (s, Cp). **HRMS ESI (m/z)**: $[M-Cl]^+$ calculated for $C_{20}H_{18}AsFe_2$, 444.93177; found, 444.93106.

Synthesis of $[Fc_2P][B(C_6F_5)_4]$ (**1P**$[B(C_6F_5)_4]$). To a solid mixture of Fc_2PCl (2P, 218 mg, 0.500 mmol) and $K[B(C_6F_5)_4]$ (359 mg, 0.500 mmol) was added CH_2Cl_2 (5 mL). The reaction mixture was stirred for 15 minutes then filtered under argon through a syringe PTFE filter. The dark-red solution was layered with hexane; dark brown needles were obtained. The solvent was decanted, and the solid was dried under vacuum. **1P**$[B(C_6F_5)_4]$ was obtained in 92% yield (460 mg).

M.p. = 138–139 °C (decomp.). **^{1}H NMR (600 MHz, CD_2Cl_2)**: δ = 5.47 (m, 4H, PCp Hβ), 4.70 (s, 10H, Cp), 4.68 (m, br, 4H, PCp Hα). **^{13}C{^{1}H} NMR (151 MHz, CD_2Cl_2)**: δ = 148.6 (d, $^1J(^{19}F-^{13}C)$ = 242 Hz, *m*-C_6F_5), 138.7 (d, $^1J(^{19}F-^{13}C)$ = 245 Hz, *p*-C_6F_5), 136.8 (d, $^1J(^{19}F-^{13}C)$ = 247 Hz, *o*-C_6F_5), 124.2 (s, br, *i*-C_6F_5), 92.2 (d, $^1J(^{31}P-^{13}C)$ = 57 Hz, P–Cp *i*-C), 83.8 (s, P–Cp Cβ), 78.5 (d, $^2J(^{31}P-^{13}C)$ = 18 Hz, P–Cp Cα), 76.0 (s, Cp). **^{31}P{^{1}H} NMR (243 MHz, CD_2Cl_2)**: δ = 183.5 (s). **^{19}F NMR (565 MHz, CD_2Cl_2)**: δ = −133.1 (s, 8F, *m*-C_6F_5), −163.3 (t, $^3J(^{19}F-^{19}F)$ = 20 Hz, 4F, *p*-C_6F_5), −167.2 (t, $^3J(^{19}F-^{19}F)$ = 19 Hz, 8F, *o*-C_6F_5). **^{11}B NMR (193 MHz, CD_2Cl_2)**: δ = −16.7 (s). **HRMS ESI (m/z)**: $[M+H_2O]^+$ calculated for $C_{20}H_{20}Fe_2OP$, 418.99450; found, 418.99413.

Synthesis of $[Fc_2As][B(C_6F_5)_4]$ (**1As**$[B(C_6F_5)_4]$). To a solid mixture of 2As (240 mg, 0.500 mmol) and $K[B(C_6F_5)_4]$ (359 mg, 0.500 mmol) was added CH_2Cl_2 (8 mL). The dark purple reaction mixture was stirred at room temperature for 15 min and afterwards was filtered through PTFE syringe filter. All the volatiles were evaporated to dryness, and the solid was washed with hexane (2×3 mL). The remaining solid was dried under vacuum; **1As**$[B(C_6F_5)_4]$ was obtained as dark purple solid (419 mg, 86%).

M.p. = 209–210 °C. **^{1}H NMR (600 MHz, CD_2Cl_2)**: δ = 5.37 (m, br, 4H, AsCp), 4.70 (s, 10H, Cp), 4.65 (m, br, 4H, AsCp). **^{13}C{^{1}H} NMR (151 MHz, CD_2Cl_2)**: δ = 148.7 (d, $^1J(^{19}F-^{13}C)$ = 241 Hz, *m*-C_6F_5), 138.8 (d, $^1J(^{19}F-^{13}C)$ = 244 Hz, *p*-C_6F_5), 136.8 (d, $^1J(^{19}F-^{13}C)$ = 245 Hz, *o*-C_6F_5), 124.5 (s, br, *i*-C_6F_5), 98.58 (s, As–Cp *i*-C), 81.9 (s, As–Cp), 78.6 (s, As–Cp), 74.8 (s, Cp). **^{19}F NMR (565 MHz, CD_2Cl_2)**: δ = −133.1 (s, 8F, *m*-C_6F_5), −163.6 (t, $^3J(^{19}F-^{19}F)$ = 20 Hz, 4F, *p*-C_6F_5), −167.4 (t, $^3J(^{19}F-^{19}F)$ = 19 Hz, 8F, *o*-C_6F_5). **^{11}B NMR (193 MHz, CD_2Cl_2)**: δ = −16.7 (s). **HRMS ESI (m/z)**: $[M]^+$ calculated for $C_{20}H_{18}AsFe_2$, 444.93181; found, 444.93124.

Synthesis of $[Fc_2Sb][B(C_6F_5)_4]$ (**1Sb**$[B(C_6F_5)_4]$). *Method A*: To a solid mixture of 3Sb (136 mg, 0.201 mmol) and $[Ph_3C][B(C_6F_5)_4]$ (186 mg, 0.202 mmol) was added CH_2Cl_2 (5 mL). The reaction mixture was stirred overnight, then the solvent evaporated. The solid was washed with a toluene/hexane mixture (V:V, 1:1. 3×6 mL), and then with hexane (1×2 mL).* After drying the solid under vacuum, **1Sb**$[B(C_6F_5)_4]$ was obtained as a black powder (183 mg, 78%).

Method B: Fc_3Sb (**3Sb**, 68 mg, 0.10 mmol) and the pentamethylcyclopentenyl cation ($[C_5Me_5H_2][B(C_6F_5)_4]$, 82 mg, 0.10 mmol) were dissolved in CH_2Cl_2 (1.5 mL). The dark red reaction mixture was stirred at room temperature for 5 min, followed by the removal of the solvent under vacuum. The solid was washed with *n*-hexane (3×3 mL, until the *n*-hexane was colorless), and subsequently dried *in vacuo*. The black powder was isolated in 84% yield (98 mg).

M.p. = 178–179 °C (decomp.). **^{1}H NMR (600 MHz, CD_2Cl_2)**: δ = 5.30 (s, br, 4H, SbCp), 4.74 (s, 10H, Cp), 4.57 (s, br, 4H, SbCp). **^{13}C{^{1}H} NMR (151 MHz, CD_2Cl_2)**: 148.0 (d, $^1J(^{19}F-^{13}C)$ = 241 Hz, *m*-C_6F_5), 138.4 (d, $^1J(^{19}F-^{13}C)$ = 244 Hz, *p*-C_6F_5), 136.3 (d, $^1J(^{19}F-^{13}C)$ = 246 Hz, *o*-C_6F_5), 123.8 (s, br, C_6F_5 *i*-C), 92.5 (s, br, Bi–Cp *i*-C), 80.7 (s, Bi–Cp), 79.7 (s, Bi–Cp), 73.0 (s, Cp). **^{19}F NMR (565 MHz, CD_2Cl_2)**: δ = −134.2 (s, 8F, *m*-C_6F_5), −164.0 (t, $^3J(^{19}F-^{19}F)$ = 20 Hz, 4F, *p*-C_6F_5), −168.3 (t, $^3J(^{19}F-^{19}F)$ = 19 Hz, 8F, *o*-C_6F_5). **^{11}B NMR (193 MHz, CD_2Cl_2)**: δ = −17.4 (s). **HRMS ESI (m/z)**: $[M]^+$ calculated for $C_{20}H_{18}Fe_2Sb$, 490.91399; found, 490.91380.

*Ph_3CFc is the side product of method *A* (isolated from the toluene washings, orange solid) for the synthesis of the compounds **1Sb**$[B(C_6F_5)_4]$ and **1Bi**$[B(C_6F_5)_4]$. Single crystals were obtained from saturated toluene solution (92% yield), and the previously unknown molecular structure is shown in the ESI, figure S63. **M.p.** = 184–185 °C. **^{1}H NMR (600 MHz, CD_2Cl_2)**: δ = 7.24 (m, 15H, Ph), 4.23 (t, $J(^1H-^1H)$ = 2 Hz, 2H, C–Cp), 3.94 (s, 5H, Cp), 3.92 (t, $J(^1H-^1H)$ = 2 Hz, 2H, C–Cp). **^{13}C{^{1}H} NMR (151 MHz, CD_2Cl_2)**: δ = 148.5 (s, C), 130.9 (s, C–Ph), 127.6 (s, C–Ph), 126.7 (s, C–Ph), 98.7 (s, C–Ph), 71.9 (s, C–Cp), 69.9 (s, C–Cp), 68.2 (s, C–Cp), 59.3 (s, C–Cp). **HRMS EI (m/z)**: $[M]^+$ calculated for $C_{29}H_{24}Fe$, 428.12225; found, 428.12219.

Synthesis of $[Fc_2Bi][B(C_6F_5)_4]$ (**1Bi**$[B(C_6F_5)_4]$). *Method A*: To a solid mixture of 3Bi (169 mg, 0.221 mmol) and $[Ph_3C][B(C_6F_5)_4]$ (204 mg, 0.221 mmol) was added CH_2Cl_2. The reaction mixture was stirred overnight, then the solvent evaporated. The solid was washed with a toluene/hexane mixture (V:V, 1:1, 3×6 mL), and then additionally with hexane (1×2 mL).* After drying the solid under vacuum, **1Bi**$[B(C_6F_5)_4]$ was obtained as black powder (247 mg, 89%).

Method B: Fc_3Bi (**3Bi**, 76 mg, 0.099 mmol) and the pentamethylcyclopentenyl cation ($[C_5Me_5H_2][B(C_6F_5)_4]$, 82 mg, 0.10 mmol) were dissolved in CH_2Cl_2 (1.5 mL). The dark red reaction mixture was stirred at room temperature for 5 min. Both the removal of the solvent under vacuum or the addition of *n*-hexane (5 mL), in order to precipitate the freshly formed cation, resulted in decomposition. Metallic bismuth precipitated, and ferrocenium ion could be identified by HRMS ESI measurements.

M.p. = 213–214 °C (decomp.). **^{1}H NMR (600 MHz, CD_2Cl_2)**: δ = 5.23 (s, br, 4H, BiCp Hβ), 4.75 (s, br, 4H, BiCp Hα), 4.69 (s, 10H, Cp). **^{13}C{^{1}H} NMR (151 MHz, CD_2Cl_2)**: 148.6 (d, $^1J(^{19}F-^{13}C)$ = 240 Hz, *m*-C_6F_5), 138.8 (d, $^1J(^{19}F-^{13}C)$ = 244 Hz, *p*-C_6F_5), 136.8 (d, $^1J(^{19}F-^{13}C)$ = 247 Hz, *o*-C_6F_5), 127.7 (s, br, Bi–Cp *i*-C), 124.4 (s, br, C_6F_5 *i*-C), 82.4 (s, Bi–Cp Cα), 81.2 (s, Bi–Cp Cβ), 71.8 (s, Cp). **^{19}F NMR (565 MHz, CD_2Cl_2)**: δ = −133.2 (s, 8F, *m*-C_6F_5), −163.6 (t, $^3J(^{19}F-^{19}F)$ = 20 Hz, 4F, *p*-C_6F_5), −167.5 (t, $^3J(^{19}F-^{19}F)$ = 19 Hz, 8F, *o*-C_6F_5). **^{11}B NMR (193 MHz, CD_2Cl_2)**: δ = −16.8 (s). **HRMS ESI (m/z)**: $[M]^+$ calculated for $C_{20}H_{18}Fe_2Bi$, 578.99058; found, 578.98966.

Attempted synthesis of $[Fc_2N][B(C_6F_5)_4]$ (1 N). Over the frozen solution of Fc_2NH (19 mg, 0.050 mmol) in 3-fluorotoluene (2 mL), a solution of $[Ph_3C][B(C_6F_5)_4]$ (46 mg, 0.050 mmol) in the same solvent was added slowly. Similar procedures were used to react the amine in 1,2-difluorobenzene and dichloromethane both at low and room temperatures. In the end the products mixture turned out to be roughly the same.

Reduction Reactions – General Procedure

Cobaltocene (0.100 mmol) and $[Fc_2E][B(C_6F_5)_4]$ (0.100 mmol; E=P (**1P**), As (**1As**), Sb (**1Sb**), Bi (**1Bi**);) were mixed together as solids, and then dissolved in CH_2Cl_2 (3 mL) at room temperature. For **1P**$[B(C_6F_5)_4]$ and **1As**$[B(C_6F_5)_4]$, the solution turned from dark red to orange, and then, after 30 min of stirring, a precipitate formed. The solvent was removed by evaporation, and the resulting orange solid was washed with MeCN (4×1 mL) to remove $[Cp_2Co][B(C_6F_5)_4]$.* After filtration, the solids were dried under reduced pressure and yielding orange powders (90–95% yield). Suitable crystals for structure determination were obtained by liquid-to-liquid layer diffusion (CH_2Cl_2/hexane), and/or crystals formed spontaneously from a saturated solution in CH_2Cl_2.

1Sb$[B(C_6F_5)_4]$ and **1Bi**$[B(C_6F_5)_4]$ decomposed, after the reduction reactions, to the corresponding metallic components, and $[Fc][B(C_6F_5)_4]$, which was confirmed by ESI HRMS.

*$[Cp_2Co][B(C_6F_5)_4]$[54] is the side product of the above-mentioned reduction reactions (isolated from the MeCN washings, yellow solid) for the synthesis of the compounds **4P** and **4As**. **M.p.** = 312 °C (decomp.). **^{1}H NMR (600 MHz, CD_2Cl_2)**: δ = 5.64 (s, 10H, Cc). **^{13}C{^{1}H} NMR (151 MHz, CD_2Cl_2)**: δ = 148.7 (d, $^1J(^{19}F–^{13}C)$ = 240 Hz, *m*-C_6F_5), 138.8 (d, $^1J(^{19}F–^{13}C)$ = 244 Hz, *p*-C_6F_5), 136.9 (d, $^1J(^{19}F–^{13}C)$ = 246 Hz, *o*-C_6F_5), 124.3 (s, br, C_6F_5 *i*-C), 85.2 (s, Cc). **^{19}F NMR (565 MHz, CD_2Cl_2)**: δ = −133.0 (s, 8F, *m*-C_6F_5), −163.5 (t, $^3J(^{19}F–^{19}F)$ = 20 Hz, 4F, *p*-C_6F_5), −167.4 (t, $^3J(^{19}F–^{19}F)$ = 20 Hz, 8F, *o*-C_6F_5). **^{11}B NMR (193 MHz, CD_2Cl_2)**: δ = −16.6 (s). **HRMS ESI (m/z)**: $[M]^+$ calculated for $C_{10}H_{10}Co$, 189.01090; found, 189.01050.

Fc_2PPFc_2 (4P)

M.p. = 242–243 °C (decomp.). **^{1}H NMR (600 MHz, CD_2Cl_2)**: δ = 4.35 (s, br, 4H, PCp), 4.25 (s, br, 4H, PCp), 4.19 (s, 20H, Cp), 4.13 (s, br, 4H, PCp), 3.87 (s, br, 4H, PCp). **^{13}C{^{1}H} NMR (151 MHz, CD_2Cl_2)**: δ = 78.3 (vt, *N* = 6 Hz, P–Cp *i*-C), 74.7 (vt, *N* = 10 Hz, P–Cp), 73.7 (vt, *N* = 11 Hz, P–Cp), 70.3 (s, P–Cp), 69.7 (s, Cp), 69.6 (t, $^3J(^{31}P–^{13}C)$ = 3 Hz, P–Cp). **^{31}P{^{1}H} NMR (243 MHz, CD_2Cl_2)**: δ = −30.5 (s). **HRMS ESI (m/z)**: $[M+O_2]^+$ calculated for $C_{40}H_{36}Fe_4O_2P_2$, 833.95826; found, 833.95570.

$Fc_2AsAsFc_2$ (4As)

M.p. = 192–193 °C (decomp). **^{1}H NMR (600 MHz, CD_2Cl_2)**: δ = 4.22 (s, br, 8H, PCp), 4.18 (s, 20H, Cp), 4.12 (s, br, 4H, PCp), 3.88 (s, br, 4H, PCp). **^{13}C{^{1}H} NMR (151 MHz, CD_2Cl_2)**: δ = 78.2 (s, As–Cp *i*-C), 74.2 (s, As–Cp), 73.6 (s, As–Cp), 70.2 (s, As–Cp), 69.5 (s, Cp), 69.5 (s, As–Cp). **HRMS ESI (m/z)**: $[M+O_2]^+$ calculated for $C_{40}H_{36}Fe_4O_2As_2$, 905.85901; found, 905.85731.

Oxidation Reactions – General Procedure

Monocation oxidations: $[Ag(C_6H_6)_3][B(C_6F_5)_4]$ (0.100 mmol) and $[Fc_2E][B(C_6F_5)_4]$ (0.100 mmol; E=P (**1P**), As (**1As**), Sb (**1Sb**), Bi (**1Bi**)) were mixed together as solids, and CH_2Cl_2 (2 mL) was added to the Schlenk flask at room temperature. The reaction mixture was stirred vigorously for 30 min, until the formation of Ag mirror was observed, and then the suspension was filtered. In the case of **1P**$[B(C_6F_5)_4]$ and **1As**$[B(C_6F_5)_4]$, the color turned from dark red to dark brown, and, respectively, to dark green. The solvent was removed by evaporation, and the resulting oil was washed with pentane until it became a solid (dark green).

Following the above-mentioned procedure, **5As[$B(C_6F_5)_4$]** was isolated in 89% yield (156 mg).

1Sb and **1Bi** decomposed, after oxidation, to the corresponding metallic components (Sb^0 and Bi^0), and $[Fc][B(C_6F_5)_4]$, which was confirmed by ESI HRMS.

X-ray crystallography. Intensity data of **1E**$[B(C_6F_5)_4]$ (E=P, As Sb, Bi), **2As** (two modifications), **4P** and **4As** were collected at 100 K on a Bruker Venture D8 diffractometer with graphite-monochromated Mo–Kα (0.7107 Å) radiation. All structures were solved by direct methods and refined based on F^2 by use of the SHELX program package as implemented in OLEX 2 version 1.5.[72] All non-hydrogen atoms were refined using anisotropic displacement parameters. Hydrogen atoms attached to carbon atoms were included in geometrically calculated positions using a riding model. Crystal and refinement data are collected in Table S3-S5. Figures were created using DIAMOND.[73] Crystallographic data for the structural analyses have been deposited with the Cambridge Crystallographic Data Centre, nos. 2381458 – 2381464. Copies of this information may be obtained free of charge from The Director, CCDC, 12 Union Road, Cambridge CB2 1EZ, UK (Fax: +44–1223–336033; e-mail: deposit@ccdc.cam.ac.uk or http://www.ccdc.cam.ac.

Computational DFT analysis. Starting from the solid-state molecular geometries of **1P**–**1Bi**, structural optimizations were conducted for **1P**–**1Bi** and **5P**–**5Bi** employing density functional theory (DFT) at the B3PW91/6–311+G(2df,p)[74,75] level of theory using Gaussian16.[76] For the Sb, and Bi atoms fully relativistic effective core potentials (Sb: ECP28MDF; Bi: ECP60MDF) and corresponding cc-pVTZ basis sets were utilized.[77] Dispersion was taken account for by the empirical dispersion correction of Grimme.[78] Normal mode (or frequency) analysis proved the structures to be local minima. The wavefunction files were used for a topological analysis of the electron density and the virial field following the Atoms-In-Molecules (AIM)[43] space-partitioning scheme (using AIM2000),[79] whereas Electron-Localizability-Indicator (ELI–D)[45] related real-space bonding descriptors were generated with DGRID-5.1 (grid step size of 0.05 a.u. for numbers, 0.15 a.u. for figures).[80] Non-covalent interaction index (NCI)[44] grids were generated with NCIplot.[81] Molecular orbitals (MO) and spin densities (SD) were extracted from the formatted checkpoint files with the cubegen subroutine of Gaussian16. Bond paths are displayed with AIM2000, ELI–D and NCI figures are displayed with MolIso,[82] MO and SD images are generated with GaussView-3.[83]

Acknowledgements

The Deutsche Forschungsgemeinschaft (DFG) is gratefully acknowledged for financial support. We thank Dorit Kemken and Dr. Thomas Dülcks for the mass spectrometry measurements. We are indebted to Prof. Franc Meyer Universität Göttingen for granting access to his Mößbauer spectrometer. Open Access funding enabled and organized by Projekt DEAL.

Conflict of Interests

The authors declare no conflict of interest.

Data Availability Statement

Figures of NMR spectra as well as crystal and refinement data are given in the supporting information. Crystallographic information files (CIF) have been deposited with the Cambridge Crystallographic Data Centre (*vide supra*). Additional results from quantum chemical calculations are given in the supporting information. The raw data that support the findings of this study are available from the corresponding authors upon reasonable request.

Keywords: Pnictogenium ions · Carbene analogues · Ferrocene · Cations · Lewis acids

[1] I. M. Riddlestone, A. Kraft, J. Schaefer, I. Krossing, *Angew. Chem. Int. Ed.* **2018**, *57*, 13982–14024.
[2] M. Cais, *Organomet. Chem. Rev.* **1966**, *1*, 435–454.
[3] S. Luoan, M. Kapon, M. Cais, F. H. Herbstein, *Angew. Chem.* **1972**, *84*, 1104–1106.

[4] M. Cais, S. Dani, F. Herbstein, M. Kapon, *J. Amer. Chem. Soc.* **1978**, *100*, 5554–5558.
[5] U. Behrens, *J. Organomet. Chem.* **1979**, *182*, 89–98.
[6] R. Gleiter, H. Schimanke, S. J. Silverio, M. Büchner, G. Huttner, *Organometallics* **1996**, *15*, 5635–5640.
[7] A. Z. Kreidlin, F. M. Dolgushin, A. I. Yanovsky, Z. A. Kerzina, P. V. Petrovskii, M. I. Rybinskaya, *J. Organomet. Chem.* **2000**, *616*, 106–111.
[8] C. Bleiholder, F. Rominger, R. Gleiter, *Organometallics* **2009**, *28*, 1014–1017.
[9] The dip angle a is defined as the angle subtended by the C–E bond vector and the plane of the cyclopentadienyl (Cp) ring and reflects the bending of E towards the iron atom
[10] A. Appel, F. Jäkle, T. Priermeier, R. Schmid, M. Wagner, *Organometallics* **1996**, *15*, 1188–1194.
[11] B. E. Carpeter, W. E. Piers, M. Parvez, G. P. A. Yap, S. J. Rettig, *Can. J. Chem.* **2001**, *79*, 857–867.
[12] M. Scheibitz, M. Bolte, J. W. Bats, H. W. H. W. Lerner, I. Nowik, R. H. Herber, A. Krapp, M. Lein, M. C. Holthausen, M. Wagner, *Chem. Eur. J.* **2005**, *11*, 584–603.
[13] L. Kaufmann, J.-M. Breunig, H. Vitze, F. Schrödel, I. Nowik, M. Pichlmaier, M. Bolte, H.-W. Lerner, R. F. Winter, R. H. Herber, M. Wagner, *Dalton Trans.* **2009**, 2940–2950.
[14] L. Köring, A. Stepen, B. Birenheide, S. Barth, M. Leskov, R. Schoch, F. Krämer, F. Breher, J. Paradies, *Angew. Chem. Int. Ed.* **2023**, *62*, e202216959.
[15] H. F. T. Klare, L. Albers, L. Süsse, S. Keess, T. Müller, M. Oestreich, *Chem. Rev.* **2021**, *121*, 5889–5985.
[16] K. Müther, R. Fröhlich, C. Mück-Lichtenfeld, S. Grimme, M. Oestreich, *J. Amer. Chem. Soc.* **2011**, *133*, 12442–12444.
[17] K. Müther, P. Hrobárik, V. Hrobáriková, M. Kaupp, M. Oestreich, *Chem. Eur. J.* **2013**, *19*, 16579–16594.
[18] S. G. Baxter, R. L. Collins, A. H. Cowley, S. F. Sena, *J. Am. Chem. Soc.* **1981**, *103*, 714–715.
[19] S. G. Baxter, R. L. Collins, A. H. Cowley, S. F. Sena, *Inorg. Chem.* **1983**, *22*, 3475–3479.
[20] M. Olaru, D. Duvinage, E. Lork, S. Mebs, J. Beckmann, *Angew. Chem. Int. Ed.* **2018**, *57*, 10080–10084.
[21] M. Olaru, S. Mebs, J. Beckmann, *Angew Chem. Int. Ed.* **2021**, *60*, 19133–19138.
[22] M. Janssen, S. Mebs, J. Beckmann, *ChemPlusChem* **2023**, e2022000429
[23] M. Olaru, A. Mischin, L. A. Malaspina, S. Mebs, J. Beckmann, *Angew. Chem. Int. Ed.* **2020**, *59*, 1581–1584.
[24] B. Bildstein, M. Malaun, H. Kopacka, K. Wurst, *Z. Naturforsch.* **1999**, *54b*, 1450–1456.
[25] Y. Suzuki, T. Sasamori, J.-D. Guo, N. Tokitoh, *Chem. Eur. J.* **2018**, *24*, 364–368.
[26] K. Iijima, K. Sugamata, P. K. Majhi, T. Sasamori, *Eur. J. Inorg. Chem.* **2024**, *27*, e202400198.
[27] D. Guillaneux, H. B. Kagan, *J. Org. Chem.* **1995**, *60*, 2502–2505.
[28] C. Förster, K. Heinze, *Z. Anorg. Allg. Chem.* **2015**,*641*, 517–520.
[29] S. J. Conway, J. C. Miller, A. D. Bond, B. P. Clark, D. E. Jane, *J. Chem. Soc., Perkin Trans.* **2002**, *1*, 1625–1627.
[30] K. Izod, P. Evans, P. G. Waddell, *Chem. Commun.* **2018**, *54*, 2526–2529.
[31] The molecular structure of Fc_2AsCl (**2As**) in presented in Figure S62.
[32] G. P. Sollott, W. R. Peterson, *J. Organomet. Chem.* **1969**, *19*, 143–159.
[33] P. Romanato, S. Duttwyler, A. Linden, K. K. Baldridge, J. S. Siegel, *J. Am. Chem. Soc.* **2010**, *132*, 7828–7829.
[34] C. Stoian, F. Al Hussein, W. R. Browne, E. Hupf, J. Beckmann, *ACS Org. Inorg. Au.* **2024**, DOI: 10.1021/acsorginorgau.4c00034.
[35] During the course of our work, a related paper was published: R. Rosales, C. P. Villamizar, R. C. R. Dymarcus, B. Anzaldo, D. Fernandez, G. Hernandez, R. Gutiérrez Pérez, P. Sharma, *Russ. J. Inorg. Chem.* **2023**, *68*, 1963–1971.
[36] J. C. W. Chien, W.-M. Tsai, M. D. Rausch, *J. Am. Chem. Soc.* **1991**, *113*, 8570–8571.
[37] E. W. Neuse, D. S. Trifan, *J. Amer. Chem. Soc.* **1962**, *84*, 1850–1856.
[38] The molecular structure of Ph_3CFc in presented in Figure S63.
[39] M. Otto, D. Scheschkewitz, T. Kato, M. M. Midland, J. B. Lambert, G. Bertrand, *Angew. Chem. Int. Ed.* **2002**, *41*, 2275–2276.
[40] J. N. Jones, A. H. Cowley, C. L. B. Macdonald, *Chem. Commun.* **2002**, 1520–1521.
[41] Although the exact mechanism remains unclear, it seems plausible that the cyclopentenyl cation $[C_5Me_5H_2][B(C_6F_5)_4]$ reacts with a neutral cyclopentene C_5Me_5H via C–H bond activation of one methyl group. The molecular structure of $[C_{10}(CH_2)Me_9H_4][B(C_6F_5)_4]$ in presented in Figure S64.
[42] J. M. Lipshultz, G. Li, A. T. Radosevich, *J. Am. Chem. Soc.* **2021**, *143*, 1699–1721.
[43] R. W. F. Bader, *Atoms in Molecules: A Quantum Theory*, Cambridge University Press: Oxford U. K., **1991**.
[44] E. R. Johnson, S. Keinan, P. Mori-Sanchez, J. Contreras-Garcia, A. J. Cohen, W. Yang, *J. Am. Chem. Soc.* **2010**, *132*, 6498–6506.
[45] M. Kohout, F. R. Wagner, Y. Grin, *Theor. Chem. Acc.* **2008**, *119*, 413–420.
[46] The qualitative results are displayed in Figures S66 and S67 and the quantitative descriptors are summarized in Table S7.
[47] Strong covalency is generally reflected by an ED value larger than 1 $eÅ^{-1}$, a negative Laplacian of the ED, the modulus of the total energy density over ED ratio $(H/\rho(r)_{bcp})$ being larger than the corresponding kinetic energy density over ED ratio $(G/\rho(r)_{bcp})$, considerable electron populations within the bonding ELI–D basin (N_{ELI}) accumulated within small basin volumes (V_{ELI}), and the largest value of ELI–D at the basins attractor position (γ_{ELI}) of all four bonds. Strong non-covalent bonding aspects are reflected by an ED value smaller than 1 $eÅ^{-1}$, a positive Laplacian, $H/\rho(r)_{bcp} < G/\rho(r)_{bcp}$, similar or less electron population accumulated within considerably larger ELI–D basin volumes, accompanied by the smallest γ_{ELI} value (notably, the adjacent lone-pair (LP) basins show similar characteristics). Weak secondary H···H contacts between the two ferrocenyl groups show a virial path and a small, flat and green NCI basin.
[48] V. Gutmann, *Coord. Chem. Rev.* **1976**, *18*, 225–255.
[49] M. Beckett, G. Strickland, *Polym. Commun.* **1996**, *37*, 4629–4631.
[50] P. Erdmann, J. Leitner, J. Schwarz, L. Greb, *ChemPhysChem* **2020**, *21*, 1–9.
[51] S. D. Waniek, C. Heine, D. Zorn, T. Lieberth, M. Lauck, C. Förster, K. Heinze, *Organometallics* **2022**, *41*, 2050–2058.
[52] A. Kütt, G. Jeschke, L. Toom, J. Nerut, C. A. Reed, *Chem. Eur. J.* **2020**, *26*, 8871–8874.
[53] A. N. Zeppuhar, D. E. Falvey, *J. Org. Chem.* **2020**, *85*, 8844–8850.
[54] The molecular structure of $[Cp_2Co][B(C_6F_5)_4]$ is presented in Figure S65.
[55] In our hands both published procedures gave product mixtures containing **4P** in lower yields. In addition, we carried out the reduction of **2P** with cobaltocene, however, this procedure also provided lower yields of **4P**.
[56] S. L. Hinchley, H. E. Robertson, K. B. Borisenko, A. R. Turner, B. F. Johnston, D. W. H. Rankin, M. Ahmadia, J. N. Jones, A. H. A. H. Cowley, *Dalton Trans.* **2004**, 2469–2476.
[57] A. Dashti-Mommertz, B. Neumüller, *Z. Anorg. Allg. Chem.* **1999**, *625*, 954–960.
[58] W. Shan, X.-Y. Yang, Y. Li, S. A. Pullarkat, P.-H. Leung, *Dalton Trans.* **2019**, *48*, 4602–4610.
[59] K. Ogawa, T. Kitagawa, S. Ishida, K. Komatsu, *Organometallics* **2005**, *24*, 4842–4844.
[60] For the monitored oxidation of **4P** and **4As**, see Figures S29–S33 and Figure S34, respectively.
[61] X. Pan, Y. Su, X. Chen, Y. Zhao, Y. Li, J. Zuo, X. Wang, *J. Amer. Chem. Soc.* **2013**, *135*, 5561–5564.
[62] On the other hand, when **4P** is protonated with one equivalent of $[C_5Me_5H_2][B(C_6F_5)_4]$, the phosphinophosphonium salt $[Fc_2PP(H)Fc_2][B(C_6F_5)_4]$ (**6P**) was isolated. Alternatively, **6P** was obtained from the reaction of the phosphenium ion **1P** with Fc_2PH.
[63] There is a very weakly intense EPR signal (Figure S60), which, however, is probably due to a paramagnetic trace impurity, which might be responsible for the width of the NMR signal .
[64] The presence of the tentatively assigned doublets in the ^{31}P NMR spectrum of aged **5P**, suggests the attack of the $[B(C_6F_5)_4]^-$ ion .
[65] R. J. LeSuer, C. Buttolph, W. E. Geiger, *Anal. Chem.* **2004**, *76*, 6395–6401.
[66] M. Herberhold, M. Ellinger, W. Kremnitz, *J. Organomet. Chem.* **1983**, *241*, 227–240.
[67] T. K. Panda, M. T. Gamer, P. W. Roesky, *Organometallics* **2003**, *4*, 877–878.
[68] T. M. Maier, S. Sandl, I. G. Shenderovych, A. Jacobi von Wangelin, J. J. Weigand, R. Wolf, *Chem. Eur. J.* **2019**, *25*, 238–245.
[69] G. R. Fulmer, A. J. M. Miller, N. H. Sherden, H. E. Gottlieb, A. Nudelman, B. M. Stoltz, J. E. Bercaw, K. I. Goldberg, *Organometallics* **2010**, *29*, 2176–2179.
[70] F. Menges, "Spectragryph – optical spectroscopy software", Version 1.2.12, **2022**, http://www.effemm2.de/spectragryph/ (accessed 09 04, 2023).

[71] E. Bill, MFIT Program; Max-Planck Institute for Chemical Energy Conversion: Mülheim/Ruhr, Germany, **2008**.
[72] O. V. Dolomanov, L. J. Bourhis, R. J. Gildea, J. A. K. Howard, H. Puschmann, *J. Appl. Crystallogr.* **2009**, *42*, 339–341.
[73] Putz, H.; Brandenburg GbR, K. Diamond—Crystal and Molecular Structure Visualization, Crystal Impact: Kreuzherrenstr. 102, 53227 Bonn, Germany, **2023**.
[74] A. D. Becke, *J. Chem. Phys.* **1993**, *98*, 5648–5652.
[75] J. P. Perdew, J. A. Chevary, S. H. Vosko, K. A. Jackson, M. R. Pederson, D. J. Singh, C. Fiolhais, *Phys. Rev. B* **1992**, *46*, 6671–6687.
[76] Gaussian 16, Revision C.01, M. J. Frisch, G. W. Trucks, H. B. Schlegel, G. E. Scuseria, M. A. Robb, J. R. Cheeseman, G. Scalmani, V. Barone, G. A. Petersson, H. Nakatsuji, X. Li, M. Caricato, A. V. Marenich, J. Bloino, B. G. Janesko, R. Gomperts, B. Mennucci, H. P. Hratchian, J. V. Ortiz, A. F. Izmaylov, J. L. Sonnenberg, D. Williams-Young, F. Ding, F. Lipparini, F. Egidi, J. Goings, B. Peng, A. Petrone, T. Henderson, D. Ranasinghe, V. G. Zakrzewski, J. Gao, N. Rega, G. Zheng, W. Liang, M. Hada, M. Ehara, K. Toyota, R. Fukuda, J. Hasegawa, M. Ishida, T. Nakajima, Y. Honda, O. Kitao, H. Nakai, T. Vreven, K. Throssell, J. A. Montgomery, Jr., J. E. Peralta, F. Ogliaro, M. J. Bearpark, J. J. Heyd, E. N. Brothers, K. N. Kudin, V. N. Staroverov, T. A. Keith, R. Kobayashi, J. Normand, K. Raghavachari, A. P. Rendell, J. C. Burant, S. S. Iyengar, J. Tomasi, M. Cossi, J. M. Millam, M. Klene, C. Adamo, R. Cammi, J. W. Ochterski, R. L. Martin, K. Morokuma, O. Farkas, J. B. Foresman, D. J. Fox, Gaussian, Inc., Wallingford CT, **2016**.
[77] K. A. Peterson, *J. Chem. Phys.* **2003**, *119*, 11099.
[78] S. Grimme, J. Anthony, S. Ehrlich, H. Krieg, *J. Chem. Phys.* **2010**, *132*, 154104.
[79] F. Biegler-Konig, J. Schonbohm, D. Bayles, *J. Comput. Chem.* **2001**, *22*, 545–559.
[80] M. Kohout, *DGRID*-4.6 Radebeul, **2015**.
[81] J. Contreras-Garcia, E. Johnson, S. Keinan, R. Chaudret, J.-P. Piquemal, D. Beratan, W. Yang, *J. Chem. Theory Comput.* **2011**, *7*, 625–632.
[82] C. B. Hubschle, P. Luger, *J. Appl. Crystallogr.* **2006**, *39*, 901–904.
[83] GaussView, Version 6.1, R. Dennington, T. A. Keith, J. M. Millam, Semichem Inc., Shawnee Mission, KS, **2016**.

Manuscript received: September 24, 2024
Accepted manuscript online: October 29, 2024
Version of record online: November 27, 2024